IEEE Open Journal of Signal Processing

Received 6 September 2023; revised 8 November 2023; accepted 9 November 2023. Date of publication 29 November 2023; date of current version 29 December 2023. The review of this article was arranged by Associate Editor Laurent Condat.

Digital Object Identifier 10.1109/OJSP.2023.3337729

Analytical Performance Assessment of 2-D Tensor ESPRIT in Terms of Physical Parameters

DAMIR RAKHIMOV (Member, IEEE), AND MARTIN HAARDT (Fellow, IEEE)

Communications Research Laboratory, Ilmenau University of Technology, 98693 Ilmenau, Germany

CORRESPONDING AUTHOR: DAMIR RAKHIMOV (email: damir.rakhimov@tu-ilmenau.de).

This work was supported in part by the German Research Foundation (DFG) under Grant 402834619 (AdAMMM, HA 2239/14-1 and ZH 640/2-1), and in part by the Open Access Publication Fund of the Technische Universität Ilmenau.

ABSTRACT In this paper, we present an analytical performance assessment of 2-D Tensor ESPRIT in terms of physical parameters. We show that the error in the r-mode depends only on two components, irrespective of the dimensionality of the problem. We obtain analytical expressions in closed form for the mean squared error (MSE) in each dimension as a function of the signal-to-noise (SNR) ratio, the array steering matrices, the number of antennas, the number of snapshots, the selection matrices, and the signal correlation. The derived expressions allow a better understanding of the difference in performance between the tensor and the matrix versions of the ESPRIT algorithm. The simulation results confirm the coincidence between the presented analytical expression and the curves obtained via Monte Carlo trials. We analyze the behavior of each of the two error components in different scenarios.

INDEX TERMS 2-D Tensor ESPRIT, harmonic retrieval, performance assessment, first-order perturbation analysis.

I. INTRODUCTION

Recently, the problem of high-resolution parameter estimation (HRPE) has re-attracted the attention of the research community in the context of next-generation mobile communications. The state-of-the-art algorithms operate commonly on multidimensional signals [1], [2]. This imposes that the corresponding theoretical analysis should encompass all the features inherent to their structure. However, despite the recognizable prominence of the topic of multidimensional HRPE, the number of publications analyzing the theoretical performance is rather limited due to the complexity of the task.

Among multiple available ways to tackle the problem of the analytical performance assessment, the first-order Taylor expansion of the spatial frequency as a function of the signal subspace has been successfully applied to compare the efficiency of various 1-D HRPE methods in [3]. Moreover, subsequently, it was extended to the analysis of multidimensional algorithms in [4], [5], [6], including those for strictly non-circular signals in [7], [8]. The current state-of-the-art methods for performance analysis of multidimensional parameter estimation techniques [4], [5], [6] rely on the high order singular value decomposition (HOSVD) and the related intermediate quantities that must be precomputed beforehand for every mode separately.

In this work, we present the performance analysis for 2-D Tensor ESPRIT in terms of physical parameters. We show that the error in the r-th mode depends only on two perturbation components irrespective of the dimensionality of the original problem. The result has lower complexity and higher readability because it does not rely on the parameters of the HOSVD or any intermediate expressions that could not be calculated directly from the physical parameters. Compared to previously reported works on perturbation analysis, we get a simpler expression that can be directly utilized to evaluate the performance and does not need to run computationally expensive Monte Carlo trials. We have chosen the 2-D case for this paper as the simplest example which admits tensor processing. However, an extension to more dimensions (R-D case) is also possible.

In this paper, we follow the same notation as in [2].

II. SYSTEM MODEL

We consider a multidimensional signal $\boldsymbol{\mathcal{X}}_{\mathrm{o}} \in \mathbb{C}^{M_1 \times M_2 \times N}$ on a two-dimensional (2-D) lattice of size $M = M_1 \times M_2$. It

contains a mixture of the d signals that are measured during N time instances. In this paper, we consider only the 2-D case ($R = 2$) while further extensions to larger dimensions are possible. Additionally, we present the expressions and the derivations only for the 1-mode, while the equations for the 2-mode can be derived accordingly following the material presented in this paper.

In the case of the 2-D harmonic retrieval problem, the noiseless received signal can be written in the following form using tensor notation [9]

$$\mathcal{X}_{\mathrm{o}} = \mathcal{A} \times_3 \boldsymbol{S}^{\mathrm{T}} = \mathcal{I}_{3,d} \times_1 \boldsymbol{A}^{(1)} \times_2 \boldsymbol{A}^{(2)} \times_3 \boldsymbol{S}^{\mathrm{T}}, \quad (1)$$

where $\mathcal{A} = \mathcal{I}_{3,d} \times_1 \boldsymbol{A}^{(1)} \times_2 \boldsymbol{A}^{(2)} \in \mathbb{C}^{M_1 \times M_2 \times d}$ is the array steering tensor, $\boldsymbol{A}^{(r)} \in \mathbb{C}^{M_r \times d}$ is the steering matrix for the r-th mode with the i-th column given as $\boldsymbol{a}_i^{(r)} = [1 \ \mathrm{e}^{j\mu_i^{(r)}} \ \cdots \ \mathrm{e}^{j(M_r-1)\mu_i^{(r)}}]^{\mathrm{T}} \in \mathbb{C}^{M_r}$, $\mu_i^{(r)} \in (-\pi, \pi]$ is the spatial frequency for the i-th source, $\forall r \in \{1, 2\}$, $\forall i \in \{1..d\}$, and $\boldsymbol{S} \in \mathbb{C}^{d \times N}$ is a matrix containing the complex-valued transmit signals.

On the other hand, the same signal and the corresponding economy-size singular value decomposition (SVD) can also be written using the conventional matrix notation as

$$\boldsymbol{X}_{\mathrm{o}} = \boldsymbol{A}\boldsymbol{S} = \boldsymbol{U}_{\mathrm{s}}\boldsymbol{\Sigma}_{\mathrm{s}}\boldsymbol{V}_{\mathrm{s}}^{\mathrm{H}} \in \mathbb{C}^{M_1 M_2 \times N}, \quad (2)$$

where $\boldsymbol{X}_{\mathrm{o}} = [\mathcal{X}_{\mathrm{o}}]_{(3)}^{\mathrm{T}}$ and $\boldsymbol{A} = [\mathcal{A}]_{(3)}^{\mathrm{T}} = \boldsymbol{A}^{(2)} \diamond \boldsymbol{A}^{(1)} \in \mathbb{C}^{M_1 M_2 \times d}$.

Usually, the available measurements are corrupted by additive noise so that the received signal can be represented as

$$\mathcal{X} = \mathcal{X}_{\mathrm{o}} + \mathcal{N} \in \mathbb{C}^{M_1 \times M_2 \times N}, \quad (3)$$

where $\mathcal{N} \in \mathbb{C}^{M_1 \times M_2 \times N}$ is the tensor with the samples of noise. At this point, we do not make any assumptions regarding the noise statistics.

Additionally, we denote the covariance matrix for the d sources as $\boldsymbol{R}_{\mathrm{s}} = \mathbb{E}\{\boldsymbol{s}\boldsymbol{s}^{\mathrm{H}}\} \in \mathbb{C}^{d \times d}$, where $\boldsymbol{s} \in \mathbb{C}^d$ is the vector of the transmitted signals at one time snapshot. While the actual covariance matrix might be unavailable for the algorithm, we can use an estimate of it that is calculated as $\hat{\boldsymbol{R}}_{\mathrm{s}} = \frac{1}{N}\boldsymbol{S}\boldsymbol{S}^{\mathrm{H}} \in \mathbb{C}^{d \times d}$.

A. HIGHER ORDER SINGULAR VALUE DECOMPOSITION (HOSVD)

ESPRIT-type algorithms rely on the information about the signal subspace to obtain estimates of the spatial frequencies. For the one-dimensional (1-D) case, the common approach is to use the singular value decomposition of $\boldsymbol{X}_{\mathrm{o}}$ to obtain this information. On the other hand, for the multidimensional case, it was proposed in [9] to use the truncated high-order singular value decomposition (HOSVD) to improve the accuracy of the parameter estimation. It represents the tensor $\mathcal{X}_{\mathrm{o}}$ in the form of a product between a dense core tensor $\mathcal{S}_{\mathrm{s}}$ and a series of factor matrices $\boldsymbol{U}_{\mathrm{s}}^{(r)}$, $\forall r \in \{1..R\}$. The corresponding core tensor can be found as

$$\mathcal{S}_{\mathrm{s}} = \mathcal{X}_{\mathrm{o}} \times_1 \boldsymbol{U}_{\mathrm{s}}^{(1)\mathrm{H}} \times_2 \boldsymbol{U}_{\mathrm{s}}^{(2)\mathrm{H}} \times_3 \boldsymbol{U}_{\mathrm{s}}^{(3)\mathrm{H}} \in \mathbb{C}^{d \times d \times d}, \quad (4)$$

where the factor matrices $\boldsymbol{U}_{\mathrm{s}}^{(r)}$, $\forall r \in \{1..R\}$ are found as the d dominant singular vectors in every mode, i.e., $[\mathcal{X}_{\mathrm{o}}]_{(1)} = \boldsymbol{U}_{\mathrm{s}}^{(1)}\boldsymbol{\Sigma}_{\mathrm{s}}^{(1)}\boldsymbol{V}_{\mathrm{s}}^{(1)\mathrm{H}}$, $[\mathcal{X}_{\mathrm{o}}]_{(2)} = \boldsymbol{U}_{\mathrm{s}}^{(2)}\boldsymbol{\Sigma}_{\mathrm{s}}^{(2)}\boldsymbol{V}_{\mathrm{s}}^{(2)\mathrm{H}}$, and $[\mathcal{X}_{\mathrm{o}}]_{(3)} = \boldsymbol{U}_{\mathrm{s}}^{(3)}\boldsymbol{\Sigma}_{\mathrm{s}}^{(3)}\boldsymbol{V}_{\mathrm{s}}^{(3)\mathrm{H}}$.

Then we can represent the original signal $\mathcal{X}_{\mathrm{o}}$ as

$$\begin{aligned}\mathcal{X}_{\mathrm{o}} &= \mathcal{S}_{\mathrm{s}} \times_1 \boldsymbol{U}_{\mathrm{s}}^{(1)} \times_2 \boldsymbol{U}_{\mathrm{s}}^{(2)} \times_3 \boldsymbol{U}_{\mathrm{s}}^{(3)} \\ &= \mathcal{X}_{\mathrm{o}} \times_1 \boldsymbol{T}^{(1)} \times_2 \boldsymbol{T}^{(2)} \times_3 \boldsymbol{T}^{(3)} \in \mathbb{C}^{M_1 \times M_2 \times N}, \end{aligned} \quad (5)$$

where

$$\boldsymbol{T}^{(r)} = \boldsymbol{U}_{\mathrm{s}}^{(r)}\boldsymbol{U}_{\mathrm{s}}^{(r)\mathrm{H}} = \boldsymbol{A}^{(r)}\left(\boldsymbol{A}^{(r)\mathrm{H}}\boldsymbol{A}^{(r)}\right)^{-1}\boldsymbol{A}^{(r)\mathrm{H}} \quad (6)$$

is the signal subspace projection matrix for the r-mode. For notational simplicity, we assume in this paper that $d < M_r$, $\forall r \in \{1..R\}$.

Additionally, we denote the signal subspace tensor as $\mathcal{U}_{\mathrm{s}} \in \mathbb{C}^{M_1 \times M_2 \times d}$. It shares the same multidimensional subspace as the array steering tensor $\mathcal{A}$ and can be written in the form of the equality $\mathcal{A} = \mathcal{U}_{\mathrm{s}} \times_3 \boldsymbol{K}$, where $\boldsymbol{K} \in \mathbb{C}^{d \times d}$ is a full rank matrix. Equivalently, it can also be written in the corresponding matrix form as $[\mathcal{A}]_{(3)}^{\mathrm{T}} = [\mathcal{U}_{\mathrm{s}}]_{(3)}^{\mathrm{T}} \cdot \boldsymbol{K}$.

Following [6] (therein Equation 24), we can write the fundamental link between the matrix signal subspace and tensor signal subspace as

$$\left[\mathcal{U}_{\mathrm{s}}\right]_{(3)}^{\mathrm{T}} = \left(\boldsymbol{T}^{(2)} \otimes \boldsymbol{T}^{(1)}\right) \cdot \boldsymbol{U}_{\mathrm{s}}. \quad (7)$$

The subspaces are equal in the noiseless case, but the estimates might differ in the presence of noise.

B. REVIEW OF 2-D TENSOR ESPRIT

The multidimensional version of the ESPRIT algorithm is based on the tensor formulation of the shift-invariance property. We provide an example for the 1-mode while the expressions for the 2-mode can be written accordingly. We start with the expression for the shift-invariance equation along the 1-mode, which can be written as

$$\mathcal{A} \times_1 \boldsymbol{J}_1^{(1)} \times_3 \boldsymbol{\Phi}^{(1)} = \mathcal{A} \times_1 \boldsymbol{J}_2^{(1)}, \quad (8)$$

where $\boldsymbol{J}_1^{(1)} \in \mathbb{R}^{(M_1-1) \times M_1}$ and $\boldsymbol{J}_2^{(1)} \in \mathbb{R}^{(M_1-1) \times M_1}$ are the selection matrices for the 1-mode. Here, we assume that the maximum overlap configuration is used [10]. The matrix $\boldsymbol{\Phi}^{(1)} = \mathrm{diag}(\mathrm{e}^{j\mu_i^{(1)}})_{i=1}^{d} \in \mathbb{C}^{d \times d}$ contains the phase differences between two subarrays in the 1-mode with information about the spatial directions towards different sources.

The shift-invariance property for the 1-mode can also be written in matrix form if we use the transpose of the 3-mode unfolding as

$$\tilde{\boldsymbol{J}}_1^{(1)} \cdot \left[\mathcal{A}\right]_{(3)}^{\mathrm{T}} \cdot \boldsymbol{\Phi}^{(1)} = \tilde{\boldsymbol{J}}_2^{(1)} \cdot \left[\mathcal{A}\right]_{(3)}^{\mathrm{T}}, \quad (9)$$

where $\tilde{\boldsymbol{J}}_1^{(1)} = (\boldsymbol{I}_{M_2} \otimes \boldsymbol{J}_1^{(1)})$ and $\tilde{\boldsymbol{J}}_2^{(1)} = (\boldsymbol{I}_{M_2} \otimes \boldsymbol{J}_2^{(1)})$ are the multidimensional selection matrices for the 1-mode.

During the estimation step, we do not know the tensor $\boldsymbol{\mathcal{A}} \in \mathbb{C}^{M_1 \times M_2 \times d}$, but we can calculate the corresponding tensor signal subspace $\boldsymbol{\mathcal{U}}_\mathrm{s}$ that is related to the steering tensor as $\boldsymbol{\mathcal{A}} = \boldsymbol{\mathcal{U}}_\mathrm{s} \times_3 \boldsymbol{K}$. Hence, we rewrite (9) as

$$\tilde{\boldsymbol{J}}_1^{(1)} \left[\boldsymbol{\mathcal{U}}_\mathrm{s}\right]_{(3)}^\mathrm{T} \underbrace{\boldsymbol{K}\boldsymbol{\Phi}^{(1)}\boldsymbol{K}^{-1}}_{\boldsymbol{\Psi}^{(1)}} = \tilde{\boldsymbol{J}}_2^{(1)} \left[\boldsymbol{\mathcal{U}}_\mathrm{s}\right]_{(3)}^\mathrm{T}. \tag{10}$$

In the next step, we estimate the matrix $\boldsymbol{\Psi}^{(1)}$ using, for example, the method of least squares as

$$\boldsymbol{\Psi}^{(1)} = \left(\tilde{\boldsymbol{J}}_1^{(1)} \left[\boldsymbol{\mathcal{U}}_\mathrm{s}\right]_{(3)}^\mathrm{T}\right)^+ \cdot \left(\tilde{\boldsymbol{J}}_2^{(1)} \left[\boldsymbol{\mathcal{U}}_\mathrm{s}\right]_{(3)}^\mathrm{T}\right). \tag{11}$$

Since the matrix $\boldsymbol{\Phi}^{(1)}$ is diagonal, we can treat the product $\boldsymbol{K}\boldsymbol{\Phi}^{(1)}\boldsymbol{K}^{-1}$ as the corresponding eigenvalue decomposition of $\boldsymbol{\Psi}^{(1)}$. As a result, we find the diagonal entries of the matrix $\boldsymbol{\Phi}^{(1)}$ through the eigenvalue decomposition of the matrix $\boldsymbol{\Psi}^{(1)} = \boldsymbol{Q}^{(1)^{-1}}\boldsymbol{\Lambda}^{(1)}\boldsymbol{Q}^{(1)}$, as the entries of the diagonal matrix $\boldsymbol{\Lambda}^{(1)} \in \mathbb{C}^{d \times d}$.

Finally, we compute the estimates of the spatial frequencies $\mu_i^{(1)}, \forall i \in \{1..d\}$ by taking the arguments of the estimated eigenvalues, i.e., $\mu_i^{(1)} = \arg(\lambda_i^{(1)})$.

Further information on the algorithm and an extension to the general R-D case can be found in [9].

III. PERTURBATIONS OF ESSENTIAL COMPONENTS FOR 2-D TENSOR ESPRIT

A. PERTURBATION OF THE SIGNAL SUBSPACE

In [11] (therein the lemma 1), it has been shown that we can represent the perturbation of a subspace as a leakage from the orthogonal subspace. For the signal and the noise subspaces, it can be written in the following way

$$\Delta\boldsymbol{U}_\mathrm{s} \approx \boldsymbol{U}_\mathrm{n}\boldsymbol{\Gamma}_\mathrm{n} \qquad \text{and} \qquad \Delta\boldsymbol{U}_\mathrm{n} \approx \boldsymbol{U}_\mathrm{s}\boldsymbol{\Gamma}_\mathrm{s}, \tag{12}$$

where the amount of the leakage is defined by the matrices $\boldsymbol{\Gamma}_\mathrm{n}$ and $\boldsymbol{\Gamma}_\mathrm{s}$. The exact expressions for the first-order approximation of the leakage matrices have been derived in [3] and are given by

$$\Delta\boldsymbol{U}_\mathrm{n} = -\boldsymbol{U}_\mathrm{s}\boldsymbol{\Sigma}_\mathrm{s}^{-1}\boldsymbol{V}_\mathrm{s}^\mathrm{H}\boldsymbol{N}^\mathrm{H}\boldsymbol{U}_\mathrm{n}, \text{ and } \Delta\boldsymbol{U}_\mathrm{s} = \boldsymbol{U}_\mathrm{n}\boldsymbol{U}_\mathrm{n}^\mathrm{H}\boldsymbol{N}\boldsymbol{V}_\mathrm{s}\boldsymbol{\Sigma}_\mathrm{s}^{-1}, \tag{13}$$

for the perturbation of the noise subspace and the signal subspace, respectively.

B. PERTURBATION OF THE SIGNAL SUBSPACE TENSOR

In [6] (therein Equation 25), it has been shown that the first-order perturbation of the HOSVD-based signal subspace estimate (7) can be written as the sum (14) shown at the bottom of this page.

We name each perturbation term and analyze further their impact on the estimation error. Concerning the performance in the 1-mode, each term has a specific meaning. The first perturbation term represents the impact of the core tensor perturbation on the performance in the 1-mode, the second perturbation term contains the influence of the perturbation in the 1-mode on the performance in the 1-mode, and the third perturbation term describes the impact of the perturbation in the 2-mode on the performance in the 1-mode that can be interpreted as a cross-mode contribution. We quantify the impact of each term on the performance of 2-D Tensor ESPRIT in the following part of the paper. Especially, we show that the cross-mode impact described by the term III is equal to 0 and can be omitted from the further consideration.

C. PERTURBATION OF THE i-TH SPATIAL FREQUENCY IN THE 1-MODE

Following [3] (therein Equation 50), we can write the perturbation of the i-th spatial frequency for the 1-mode as in (15) shown at the bottom of this page, where $\boldsymbol{e}_i \in \mathbb{R}^d$ is the i-th column of the identity matrix $\boldsymbol{I}_d \in \mathbb{R}^{d \times d}$. We denote the left part of the argument of the imaginary part in (15) as

$$\left[\boldsymbol{\mathcal{L}}_i^{(1)}\right]_{(3)} = \boldsymbol{e}_i^\mathrm{T}\left(\left(\tilde{\boldsymbol{J}}_2^{(1)}\boldsymbol{A}\right)^+ \tilde{\boldsymbol{J}}_2^{(1)} - \left(\tilde{\boldsymbol{J}}_1^{(1)}\boldsymbol{A}\right)^+ \tilde{\boldsymbol{J}}_1^{(1)}\right) \tag{16}$$

and assume that it represents the 3-mode unfolding of a tensor $\boldsymbol{\mathcal{L}}_i^{(1)} \in \mathbb{C}^{M_1 \times M_2 \times 1}$. Additionally, we introduce an auxiliary variable $\boldsymbol{\alpha}_i^{(1)} = [\boldsymbol{\mathcal{L}}_i^{(1)}]_{(3)}$ that we use further in the paper. We derive the tensor structure of the tensor $\boldsymbol{\mathcal{L}}_i^{(1)}$ in the next subsection. This substitution allows us to shorten the notation and write (15) as

$$\Delta\mu_i^{(1)} = \mathrm{Im}\left(\left[\boldsymbol{\mathcal{L}}_i^{(1)}\right]_{(3)} \cdot \left[\Delta\boldsymbol{\mathcal{U}}_\mathrm{s}\right]_{(3)}^\mathrm{T} \cdot \boldsymbol{K}\boldsymbol{e}_i\right). \tag{17}$$

Which we can rewrite as in (18) shown at the bottom of the next page, if we insert the definition of the perturbation for the signal subspace tensor (14) into (17). As we can see, the resulting perturbation of the spatial frequency $\mu_i^{(1)}$ depends

$$\left[\Delta\boldsymbol{\mathcal{U}}_\mathrm{s}\right]_{(3)}^\mathrm{T} = \underbrace{\left(\boldsymbol{T}^{(2)} \otimes \boldsymbol{T}^{(1)}\right) \cdot \Delta\boldsymbol{U}_\mathrm{s}}_{\left[\Delta\boldsymbol{\mathcal{U}}_{\mathrm{s,I}}\right]_{(3)}^\mathrm{T}} + \underbrace{\left(\boldsymbol{I}_{M_2} \otimes \Delta\boldsymbol{U}_\mathrm{s}^{(1)}\boldsymbol{U}_\mathrm{s}^{(1)^\mathrm{H}}\right) \cdot \boldsymbol{U}_\mathrm{s}}_{\left[\Delta\boldsymbol{\mathcal{U}}_{\mathrm{s,II}}\right]_{(3)}^\mathrm{T}} + \underbrace{\left(\Delta\boldsymbol{U}_\mathrm{s}^{(2)}\boldsymbol{U}_\mathrm{s}^{(2)^\mathrm{H}} \otimes \boldsymbol{I}_{M_1}\right) \cdot \boldsymbol{U}_\mathrm{s}}_{\left[\Delta\boldsymbol{\mathcal{U}}_{\mathrm{s,III}}\right]_{(3)}^\mathrm{T}} \tag{14}$$

$$\Delta\mu_i^{(1)} = \mathrm{Im}\left(\boldsymbol{e}_i^\mathrm{T}\left(\left(\tilde{\boldsymbol{J}}_2^{(1)}\boldsymbol{A}\right)^+ \tilde{\boldsymbol{J}}_2^{(1)} - \left(\tilde{\boldsymbol{J}}_1^{(1)}\boldsymbol{A}\right)^+ \tilde{\boldsymbol{J}}_1^{(1)}\right) \cdot \left[\Delta\boldsymbol{\mathcal{U}}_\mathrm{s}\right]_{(3)}^\mathrm{T} \cdot \boldsymbol{K}\boldsymbol{e}_i\right) \tag{15}$$

on the three components. Further in the paper, we analyze the impact of each of them.

Additionally, we should mention the pairing of the parameters across the dimensions and its impact on the performance of the algorithm. We assume that the proper pairing is ensured via a joint eigenvalue decomposition (JEVD) of all the matrices $\boldsymbol{\Phi}^{(r)}$, $\forall r \in 1..R$. However, we do not include the performance analysis of this step in the paper since for high SNRs, the perturbation of the EVD in the r-mode is dominated by the perturbation of eigenvalues, and the perturbation of the common set of eigenvectors can be excluded from the analysis [6] (therein Equation 31).

D. TENSOR STRUCTURE OF $\mathcal{L}_i^{(1)}$

We start deriving the tensor formulation of $\mathcal{L}_i^{(1)}$ by writing explicitly the expression

$$\boldsymbol{e}_i^{\mathrm{T}} \left(\tilde{\boldsymbol{J}}_2^{(1)} \boldsymbol{A}\right)^{+} \tilde{\boldsymbol{J}}_2^{(1)} = \boldsymbol{e}_i^{\mathrm{T}} \left(\boldsymbol{A}^{(2)} \diamond \boldsymbol{J}_2^{(1)} \boldsymbol{A}^{(1)}\right)^{+} \cdot \left(\boldsymbol{I}_{M_2} \otimes \boldsymbol{J}_2^{(1)}\right), \quad (19)$$

where we used the property for the mixed product $(\boldsymbol{A} \otimes \boldsymbol{B})(\boldsymbol{C} \diamond \boldsymbol{D}) = \boldsymbol{AC} \diamond \boldsymbol{BD}$. Taking into account the expression for the pseudoinverse of a Khatri-Rao product $(\boldsymbol{C} \diamond \boldsymbol{D})^{+} = (\boldsymbol{C}^{\mathrm{H}}\boldsymbol{C} \odot \boldsymbol{D}^{\mathrm{H}}\boldsymbol{D})^{-1}(\boldsymbol{C} \diamond \boldsymbol{D})^{\mathrm{H}}$, we can write (19) as

$$\begin{aligned} &\boldsymbol{e}_i^{\mathrm{T}} \left(\boldsymbol{A}^{(2)\mathrm{H}}\boldsymbol{A}^{(2)} \odot \boldsymbol{A}^{(1)\mathrm{H}} \boldsymbol{J}_2^{(1)\mathrm{T}} \boldsymbol{J}_2^{(1)} \boldsymbol{A}^{(1)}\right)^{-1} \\ &\quad \cdot \left(\boldsymbol{A}^{(2)} \diamond \boldsymbol{J}_2^{(1)} \boldsymbol{A}^{(1)}\right)^{\mathrm{H}} \left(\boldsymbol{I}_{M_2} \otimes \boldsymbol{J}_2^{(1)}\right) \\ &= \boldsymbol{e}_i^{\mathrm{T}} \boldsymbol{\Xi}_2^{(1)-1} \left(\boldsymbol{A}^{(2)*} \diamond \boldsymbol{J}_2^{(1)\mathrm{T}} \boldsymbol{J}_2^{(1)} \boldsymbol{A}^{(1)*}\right)^{\mathrm{T}}, \end{aligned} \quad (20)$$

where $\boldsymbol{\Xi}_2^{(1)} = \boldsymbol{A}^{(2)\mathrm{H}}\boldsymbol{A}^{(2)} \odot \boldsymbol{A}^{(1)\mathrm{H}} \boldsymbol{J}_2^{(1)\mathrm{T}} \boldsymbol{J}_2^{(1)} \boldsymbol{A}^{(1)}$. The whole expression can be viewed as the 3-mode unfolding of a tensor with the following canonical polyadic structure [12] (therein the Section 3)

$$\mathcal{I}_{3,d} \times_1 \boldsymbol{J}_2^{(1)\mathrm{T}} \boldsymbol{J}_2^{(1)} \boldsymbol{A}^{(1)*} \times_2 \boldsymbol{A}^{(2)*} \times_3 \boldsymbol{e}_i^{\mathrm{T}} \boldsymbol{\Xi}_2^{(1)-1}. \quad (21)$$

Combining this result with the analogous expressions for the second part of $[\mathcal{L}_i^{(1)}]_{(3)}$ namely $\boldsymbol{e}_i^{\mathrm{T}}(\tilde{\boldsymbol{J}}_1^{(1)}\boldsymbol{A})^{+}\tilde{\boldsymbol{J}}_1^{(1)}$, we can represent the tensor $\mathcal{L}_i^{(1)}$ as the difference of two tensors

$$\begin{aligned} \mathcal{L}_i^{(1)} = &\mathcal{I}_{3,d} \times_1 \boldsymbol{J}_2^{(1)\mathrm{T}} \boldsymbol{J}_2^{(1)} \boldsymbol{A}^{(1)*} \times_2 \boldsymbol{A}^{(2)*} \times_3 \boldsymbol{e}_i^{\mathrm{T}} \boldsymbol{\Xi}_2^{(1)-1} \\ &- \mathcal{I}_{3,d} \times_1 \boldsymbol{J}_1^{(1)\mathrm{T}} \boldsymbol{J}_1^{(1)} \boldsymbol{A}^{(1)*} \times_2 \boldsymbol{A}^{(2)*} \times_3 \boldsymbol{e}_i^{\mathrm{T}} \boldsymbol{\Xi}_1^{(1)-1}, \end{aligned} \quad (22)$$

where $\boldsymbol{\Xi}_2^{(1)} = \boldsymbol{A}^{(2)\mathrm{H}}\boldsymbol{A}^{(2)} \odot \boldsymbol{A}^{(1)\mathrm{H}} \boldsymbol{J}_2^{(1)\mathrm{T}} \boldsymbol{J}_2^{(1)} \boldsymbol{A}^{(1)}$ and $\boldsymbol{\Xi}_1^{(1)} = \boldsymbol{A}^{(2)\mathrm{H}}\boldsymbol{A}^{(2)} \odot \boldsymbol{A}^{(1)\mathrm{H}} \boldsymbol{J}_1^{(1)\mathrm{T}} \boldsymbol{J}_1^{(1)} \boldsymbol{A}^{(1)}$.

This concludes the tensor formulation of $\mathcal{L}_i^{(1)}$.

IV. DECOMPOSITION OF ESTIMATION ERROR

In this section, we show the impact of various subspace perturbation terms on the resulting performance and derive the expressions for the error of each perturbation term in (14) in terms of physical parameters.

A. IMPACT OF THE FIRST PERTURBATION TERM

First, we consider the perturbation term I in (14) that is given by

$$\left[\Delta \mathcal{U}_{\mathrm{s,I}}\right]_{(3)}^{\mathrm{T}} = \left(\boldsymbol{T}^{(2)} \otimes \boldsymbol{T}^{(1)}\right) \cdot \Delta \boldsymbol{U}_{\mathrm{s}}, \quad (23)$$

while the subspace perturbation $\Delta \boldsymbol{U}_{\mathrm{s}}$ can be written as

$$\Delta \boldsymbol{U}_{\mathrm{s}} = \boldsymbol{U}_{\mathrm{n}} \boldsymbol{U}_{\mathrm{n}}^{\mathrm{H}} \left[\boldsymbol{\mathcal{N}}\right]_{(3)}^{\mathrm{T}} \boldsymbol{V}_{\mathrm{s}} \boldsymbol{\Sigma}_{\mathrm{s}}^{-1}. \quad (24)$$

If we insert the (23) and (24) in the expression (18) we can write the first component of the perturbation of the spatial frequency $\mu_i^{(1)}$ as in (25) shown at the bottom of this page.

We can drop the projection onto the left-nullspace $\boldsymbol{U}_{\mathrm{n}}\boldsymbol{U}_{\mathrm{n}}^{\mathrm{H}}$ since

$$\begin{aligned} &\left[\mathcal{L}_i^{(1)}\right]_{(3)} \left(\boldsymbol{T}^{(2)} \otimes \boldsymbol{T}^{(1)}\right) \boldsymbol{A} \\ &\quad = \boldsymbol{e}_i^{\mathrm{T}} \left(\left(\tilde{\boldsymbol{J}}_2^{(1)} \boldsymbol{A}\right)^{+} \tilde{\boldsymbol{J}}_2^{(1)} \boldsymbol{A} - \left(\tilde{\boldsymbol{J}}_1^{(1)} \boldsymbol{A}\right)^{+} \tilde{\boldsymbol{J}}_1^{(1)} \boldsymbol{A}\right) \\ &\quad = \boldsymbol{e}_i^{\mathrm{T}} \left(\boldsymbol{I}_d - \boldsymbol{I}_d\right) = \boldsymbol{0}, \end{aligned} \quad (26)$$

which means that the left part already belongs to the left-nullspace of the steering matrix $\boldsymbol{A}$, so we can omit another projection. Additionally, if we consider the right part of the expression (25), it can be rewritten as

$$\begin{aligned} \boldsymbol{V}_{\mathrm{s}} \boldsymbol{\Sigma}_{\mathrm{s}}^{-1} \boldsymbol{K} \boldsymbol{e}_i &= \boldsymbol{V}_{\mathrm{s}} \boldsymbol{\Sigma}_{\mathrm{s}}^{-1} \boldsymbol{U}_{\mathrm{s}}^{\mathrm{H}} \cdot \boldsymbol{U}_{\mathrm{s}} \boldsymbol{K} \cdot \boldsymbol{e}_i \\ &= \boldsymbol{X}_{\mathrm{o}}^{+} \cdot \boldsymbol{A} \cdot \boldsymbol{e}_i = \left(\boldsymbol{AS}\right)^{+} \boldsymbol{A} \boldsymbol{e}_i = \boldsymbol{S}^{+} \boldsymbol{e}_i. \end{aligned} \quad (27)$$

To shorten the notation, we introduce the auxiliary variables $\boldsymbol{\alpha}_{i,\mathrm{I}}^{(1)} \in \mathbb{C}^{M_1 M_2}$ and $\boldsymbol{\beta}_{i,\mathrm{I}}^{(1)} \in \mathbb{C}^{N}$ given by

$$\boldsymbol{\alpha}_{i,\mathrm{I}}^{(1)\mathrm{T}} = \left[\mathcal{L}_i^{(1)}\right]_{(3)} \left(\boldsymbol{T}^{(2)} \otimes \boldsymbol{T}^{(1)}\right) \text{ and } \boldsymbol{\beta}_{i,\mathrm{I}}^{(1)} = \boldsymbol{S}^{+} \boldsymbol{e}_i. \quad (28)$$

$$\Delta \mu_i^{(1)} = \underbrace{\mathrm{Im}\left(\left[\mathcal{L}_i^{(1)}\right]_{(3)} \left[\Delta \mathcal{U}_{\mathrm{s,I}}\right]_{(3)}^{\mathrm{T}} \boldsymbol{K} \boldsymbol{e}_i\right)}_{\Delta \mu_{i,\mathrm{I}}^{(1)}} + \underbrace{\mathrm{Im}\left(\left[\mathcal{L}_i^{(1)}\right]_{(3)} \left[\Delta \mathcal{U}_{\mathrm{s,II}}\right]_{(3)}^{\mathrm{T}} \boldsymbol{K} \boldsymbol{e}_i\right)}_{\Delta \mu_{i,\mathrm{II}}^{(1)}} + \underbrace{\mathrm{Im}\left(\left[\mathcal{L}_i^{(1)}\right]_{(3)} \left[\Delta \mathcal{U}_{\mathrm{s,III}}\right]_{(3)}^{\mathrm{T}} \boldsymbol{K} \boldsymbol{e}_i\right)}_{\Delta \mu_{i,\mathrm{III}}^{(1)}} \quad (18)$$

$$\Delta \mu_{i,\mathrm{I}}^{(1)} = \mathrm{Im}\left(\left[\mathcal{L}_i^{(1)}\right]_{(3)} \left(\boldsymbol{T}^{(2)} \otimes \boldsymbol{T}^{(1)}\right) \boldsymbol{U}_{\mathrm{n}} \boldsymbol{U}_{\mathrm{n}}^{\mathrm{H}} \left[\boldsymbol{\mathcal{N}}\right]_{(3)}^{\mathrm{T}} \boldsymbol{V}_{\mathrm{s}} \boldsymbol{\Sigma}_{\mathrm{s}}^{-1} \boldsymbol{K} \boldsymbol{e}_i\right) \quad (25)$$

It allows us to rewrite (25) as

$$\Delta\mu_{i,\mathrm{I}}^{(1)} = \mathrm{Im}\left(\boldsymbol{\alpha}_{i,\mathrm{I}}^{(1)\mathrm{T}}\left[\boldsymbol{\mathcal{N}}\right]_{(3)}^{\mathrm{T}}\boldsymbol{\beta}_{i,\mathrm{I}}^{(1)}\right) = \mathrm{Im}\left(\left(\boldsymbol{\beta}_{i,\mathrm{I}}^{(1)}\otimes\boldsymbol{\alpha}_{i,\mathrm{I}}^{(1)}\right)^{\mathrm{T}}\mathrm{vec}\left\{\left[\boldsymbol{\mathcal{N}}\right]_{(3)}^{\mathrm{T}}\right\}\right), \tag{29}$$

where we use the property for the vectorization of the product of three matrices $\mathrm{vec}\{\boldsymbol{AXB}\} = (\boldsymbol{B}^{\mathrm{T}}\otimes\boldsymbol{A})\mathrm{vec}\{\boldsymbol{X}\}$ in order to isolate the noise component for the subsequent statistical analysis.

B. IMPACT OF THE SECOND PERTURBATION TERM

Secondly, we consider the perturbation term II in (14) that is given by

$$\left[\Delta\boldsymbol{\mathcal{U}}_{\mathrm{s,II}}\right]_{(3)}^{\mathrm{T}} = \left(\boldsymbol{I}_{M_2}\otimes\Delta\boldsymbol{U}_{\mathrm{s}}^{(1)}\boldsymbol{U}_{\mathrm{s}}^{(1)\mathrm{H}}\right)\cdot\boldsymbol{U}_{\mathrm{s}} \tag{30}$$

and the corresponding perturbation in the 1-mode

$$\Delta\boldsymbol{U}_{\mathrm{s}}^{(1)} = \boldsymbol{U}_{\mathrm{n}}^{(1)}\boldsymbol{U}_{\mathrm{n}}^{(1)\mathrm{H}}\left[\boldsymbol{\mathcal{N}}\right]_{(1)}\boldsymbol{V}_{\mathrm{s}}^{(1)}\boldsymbol{\Sigma}_{\mathrm{s}}^{(1)-1}. \tag{31}$$

After inserting (30) into (18), the corresponding perturbation of the spatial frequency can be written as

$$\Delta\mu_{i,\mathrm{II}}^{(1)} = \mathrm{Im}\left(\left[\boldsymbol{\mathcal{L}}_i^{(1)}\right]_{(3)}\left(\boldsymbol{I}_{M_2}\otimes\Delta\boldsymbol{U}_{\mathrm{s}}^{(1)}\boldsymbol{U}_{\mathrm{s}}^{(1)\mathrm{H}}\right)\boldsymbol{A}\boldsymbol{e}_i\right) = \mathrm{Im}\left(\left[\boldsymbol{\mathcal{L}}_i^{(1)}\right]_{(3)}\left(\left(\boldsymbol{A}^{(2)}\boldsymbol{e}_i\right)^{\mathrm{T}}\otimes\left(\Delta\boldsymbol{U}_{\mathrm{s}}^{(1)}\boldsymbol{U}_{\mathrm{s}}^{(1)\mathrm{H}}\boldsymbol{A}^{(1)}\boldsymbol{e}_i\right)^{\mathrm{T}}\right)^{\mathrm{T}}\right), \tag{32}$$

where we take into account that $\boldsymbol{U}_{\mathrm{s}}\boldsymbol{K} = \boldsymbol{A}$ and $\boldsymbol{A}\boldsymbol{e}_i = \boldsymbol{A}^{(2)}\boldsymbol{e}_i\otimes\boldsymbol{A}^{(1)}\boldsymbol{e}_i$. We can consider the expression (32) as the 3-mode unfolding of the matrix-tensor product of the tensor $\boldsymbol{\mathcal{L}}_i^{(1)}$ along the 1-mode and the 2-mode that can be written in the form of a Tucker decomposition as

$$\Delta\mu_{i,\mathrm{II}}^{(1)} = \mathrm{Im}\left(\boldsymbol{\mathcal{L}}_i^{(1)}\times_1\left(\Delta\boldsymbol{U}_{\mathrm{s}}^{(1)}\boldsymbol{U}_{\mathrm{s}}^{(1)\mathrm{H}}\boldsymbol{A}^{(1)}\boldsymbol{e}_i\right)^{\mathrm{T}}\times_2\left(\boldsymbol{A}^{(2)}\boldsymbol{e}_i\right)^{\mathrm{T}}\right).$$

Furthermore, we can use the transpose of the 1-mode unfolding of this tensor to isolate the perturbation term at the subsequent steps. We can do this since the resulting value is a scalar independent of the specific unfolding we use to calculate it.

$$\Delta\mu_{i,\mathrm{II}}^{(1)} = \mathrm{Im}\left(\boldsymbol{e}_i^{\mathrm{T}}\boldsymbol{A}^{(2)\mathrm{T}}\left[\boldsymbol{\mathcal{L}}_i^{(1)}\right]_{(1)}^{\mathrm{T}}\Delta\boldsymbol{U}_{\mathrm{s}}^{(1)}\boldsymbol{U}_{\mathrm{s}}^{(1)\mathrm{H}}\boldsymbol{A}^{(1)}\boldsymbol{e}_i\right). \tag{33}$$

Next, we can rewrite the projection onto the left-nullspace of the matrix $\boldsymbol{A}^{(1)}$ as $\boldsymbol{U}_{\mathrm{n}}^{(1)}\boldsymbol{U}_{\mathrm{n}}^{(1)\mathrm{H}} = \boldsymbol{I}_{M_1} - \boldsymbol{T}^{(1)}$. Then, we insert (31) into (33) and rewrite the right part of the result as

$$\boldsymbol{V}_{\mathrm{s}}^{(1)}\boldsymbol{\Sigma}_{\mathrm{s}}^{(1)-1}\boldsymbol{U}_{\mathrm{s}}^{(1)\mathrm{H}}\boldsymbol{A}^{(1)}\boldsymbol{e}_i = \left[\boldsymbol{\mathcal{X}}\right]_{(1)}^{+}\boldsymbol{A}^{(1)}\boldsymbol{e}_i = \left(\boldsymbol{A}^{(1)}\left(\boldsymbol{S}^{\mathrm{T}}\diamond\boldsymbol{A}^{(2)}\right)^{\mathrm{T}}\right)^{+}\boldsymbol{A}^{(1)}\boldsymbol{e}_i = \left(\left(\boldsymbol{S}^{\mathrm{T}}\diamond\boldsymbol{A}^{(2)}\right)^{\mathrm{T}}\right)^{+}\boldsymbol{e}_i. \tag{34}$$

To simplify the notation we introduce the auxiliary variables $\boldsymbol{\alpha}_{i,\mathrm{II}}^{(1)}\in\mathbb{C}^{M_1}$, and $\boldsymbol{\beta}_{i,\mathrm{II}}^{(1)}\in\mathbb{C}^{M_2N}$ that are equal to

$$\boldsymbol{\alpha}_{i,\mathrm{II}}^{(1)\mathrm{T}} = \boldsymbol{e}_i^{\mathrm{T}}\frac{1}{\sqrt{M_2}}\boldsymbol{A}^{(2)\mathrm{T}}\left[\boldsymbol{\mathcal{L}}_i^{(1)}\right]_{(1)}\left(\boldsymbol{I}_{M_1} - \boldsymbol{T}^{(1)}\right), \tag{35}$$

$$\boldsymbol{\beta}_{i,\mathrm{II}}^{(1)\mathrm{T}} = \boldsymbol{e}_i^{\mathrm{T}}\left(\boldsymbol{S}^{\mathrm{T}}\diamond\frac{1}{\sqrt{M_2}}\boldsymbol{A}^{(2)}\right)^{+}. \tag{36}$$

The resulting impact of the second perturbation term on the error can be described by the expression

$$\Delta\mu_{i,\mathrm{II}}^{(1)} = \mathrm{Im}\left(\boldsymbol{\alpha}_{i,\mathrm{II}}^{(1)\mathrm{T}}\left[\boldsymbol{\mathcal{N}}\right]_{(1)}\boldsymbol{\beta}_{i,\mathrm{II}}^{(1)}\right) = \mathrm{Im}\left(\left(\boldsymbol{\beta}_{i,\mathrm{II}}^{(1)}\otimes\boldsymbol{\alpha}_{i,\mathrm{II}}^{(1)}\right)^{\mathrm{T}}\mathrm{vec}\left\{\left[\boldsymbol{\mathcal{N}}\right]_{(1)}\right\}\right). \tag{37}$$

C. IMPACT OF THE THIRD PERTURBATION TERM

Finally, we show that the impact of the perturbation in the 2-mode on the performance in the 1-mode is equal to 0. We consider the perturbation term III in (14) that is given by

$$\left[\Delta\boldsymbol{\mathcal{U}}_{\mathrm{s,III}}\right]_{(3)}^{\mathrm{T}} = \left(\Delta\boldsymbol{U}_{\mathrm{s}}^{(2)}\boldsymbol{U}_{\mathrm{s}}^{(2)\mathrm{H}}\otimes\boldsymbol{I}_{M_1}\right)\cdot\boldsymbol{U}_{\mathrm{s}} \tag{38}$$

and the corresponding perturbation in the 2-mode

$$\Delta\boldsymbol{U}_{\mathrm{s}}^{(2)} = \boldsymbol{U}_{\mathrm{n}}^{(2)}\boldsymbol{U}_{\mathrm{n}}^{(2)\mathrm{H}}\left[\boldsymbol{\mathcal{N}}\right]_{(2)}\boldsymbol{V}_{\mathrm{s}}^{(2)}\boldsymbol{\Sigma}_{\mathrm{s}}^{(2)-1}. \tag{39}$$

Then we insert (38) into the third term of the expression (18)

$$\Delta\mu_{i,\mathrm{III}}^{(1)} = \mathrm{Im}\left(\left[\boldsymbol{\mathcal{L}}_i^{(1)}\right]_{(3)}\left(\Delta\boldsymbol{U}_{\mathrm{s}}^{(2)}\boldsymbol{U}_{\mathrm{s}}^{(2)\mathrm{H}}\otimes\boldsymbol{I}_{M_1}\right)\boldsymbol{A}\boldsymbol{e}_i\right) = \mathrm{Im}\left(\left[\boldsymbol{\mathcal{L}}_i^{(1)}\right]_{(3)}\left(\left(\Delta\boldsymbol{U}_{\mathrm{s}}^{(2)}\boldsymbol{U}_{\mathrm{s}}^{(2)\mathrm{H}}\boldsymbol{A}^{(2)}\boldsymbol{e}_i\right)^{\mathrm{T}}\otimes\left(\boldsymbol{A}^{(1)}\boldsymbol{e}_i\right)^{\mathrm{T}}\right)^{\mathrm{T}}\right), \tag{40}$$

where we also take into account that $\boldsymbol{U}_{\mathrm{s}}\boldsymbol{K} = \boldsymbol{A}$ and $\boldsymbol{A}\boldsymbol{e}_i = \boldsymbol{A}^{(2)}\boldsymbol{e}_i\otimes\boldsymbol{A}^{(1)}\boldsymbol{e}_i$.

Considering the derived tensor structure for $[\boldsymbol{\mathcal{L}}_i^{(1)}]_{(3)}$ the argument of the imaginary part in (40) can be written in the form of a CP decomposition as in (41) shown at the bottom of this page, and it is equal to 0.

$$\boldsymbol{\mathcal{I}}_{3,d}\times_1\boldsymbol{e}_i^{\mathrm{T}}\boldsymbol{A}^{(1)\mathrm{T}}\boldsymbol{J}_2^{(1)\mathrm{T}}\boldsymbol{J}_2^{(1)}\boldsymbol{A}^{(1)*}\times_2\left(\boldsymbol{A}^{(2)\mathrm{H}}\Delta\boldsymbol{U}_{\mathrm{s}}^{(2)}\boldsymbol{U}_{\mathrm{s}}^{(2)\mathrm{H}}\boldsymbol{A}^{(2)}\boldsymbol{e}_i\right)^{\mathrm{T}}\times_3\boldsymbol{e}_i^{\mathrm{T}}\boldsymbol{\Xi}_2^{(1)-1} - \boldsymbol{\mathcal{I}}_{3,d}\times_1\boldsymbol{e}_i^{\mathrm{T}}\boldsymbol{A}^{(1)\mathrm{T}}\boldsymbol{J}_1^{(1)\mathrm{T}}\boldsymbol{J}_1^{(1)}\boldsymbol{A}^{(1)*}\times_2\left(\boldsymbol{A}^{(2)\mathrm{H}}\Delta\boldsymbol{U}_{\mathrm{s}}^{(2)}\boldsymbol{U}_{\mathrm{s}}^{(2)\mathrm{H}}\boldsymbol{A}^{(2)}\boldsymbol{e}_i\right)^{\mathrm{T}}\times_3\boldsymbol{e}_i^{\mathrm{T}}\boldsymbol{\Xi}_1^{(1)-1} = 0 \tag{41}$$

This can be explicitly shown if we consider the product $\boldsymbol{A}^{(2)\mathrm{H}}\Delta\boldsymbol{U}_{\mathrm{s}}^{(2)} \approx \boldsymbol{K}^{(2)\mathrm{H}}\boldsymbol{U}_{\mathrm{s}}^{(2)\mathrm{H}}\boldsymbol{U}_{\mathrm{n}}^{(2)}\boldsymbol{\Gamma}_{\mathrm{n}} = \boldsymbol{0}$, where the signal subspace perturbation is defined in (13) and $\boldsymbol{K}^{(2)} \in \mathbb{C}^{d\times d}$ is a full rank matrix. It brings us to the conclusion that $\Delta\mu_{i,\mathrm{III}}^{(1)} = 0$. It means that the impact of the perturbation in the 2-mode on the performance in the 1-mode, and vice versa, can be neglected.

D. DISCUSSION

We can observe that the perturbation of the i-th spatial frequency in the r-th mode depends only on two components (29) and (37) irrespective of the dimensionality of the system model. The first component (29) comes from the perturbation of the signal subspace, and the second component (37) appears due to the perturbation of the corresponding projection matrix.

V. MEAN SQUARED ERROR AND STATISTICAL ANALYSIS

A. MEAN SQUARED ERROR

In this section, we continue the analysis of the performance of the multidimensional ESPRIT-type algorithms and derive the expression for the mean squared error (MSE) of the i-th source in the 1-mode.

The MSE of the i-th source in the 1-mode can be written as

$$\begin{aligned}\mathbb{E}\left\{\left(\Delta\mu_{i}^{(1)}\right)^2\right\} &= \mathbb{E}\left\{\left(\Delta\mu_{i,\mathrm{I}}^{(1)} + \Delta\mu_{i,\mathrm{II}}^{(1)}\right)^2\right\} \\ &= \mathbb{E}\left\{\left(\Delta\mu_{i,\mathrm{I}}^{(1)}\right)^2\right\} + \mathbb{E}\left\{\left(\Delta\mu_{i,\mathrm{II}}^{(1)}\right)^2\right\} \\ &\quad + 2\cdot\mathbb{E}\left\{\Delta\mu_{i,\mathrm{I}}^{(1)}\Delta\mu_{i,\mathrm{II}}^{(1)}\right\}, \end{aligned} \tag{42}$$

where the first two terms correspond to the variances of each perturbation term, and the last component represents the correlation between the perturbation terms (29) and (37). Our simulation results show that for practical problems, we can neglect the correlation component and consider the perturbation terms $\Delta\mu_{i,\mathrm{I}}^{(1)}$ and $\Delta\mu_{i,\mathrm{II}}^{(1)}$ as uncorrelated.

We start with $\mathbb{E}\{(\Delta\mu_{i,\mathrm{I}}^{(1)})^2\}$ that can be written as

$$\begin{aligned}\mathbb{E}\left\{\left(\Delta\mu_{i,\mathrm{I}}^{(1)}\right)^2\right\} &= \frac{1}{2}\left(\boldsymbol{\beta}_{i,\mathrm{I}}^{(1)}\otimes\boldsymbol{\alpha}_{i,\mathrm{I}}^{(1)}\right)^{\mathrm{H}}\boldsymbol{R}_{\mathrm{n}}^{*}\left(\boldsymbol{\beta}_{i,\mathrm{I}}^{(1)}\otimes\boldsymbol{\alpha}_{i,\mathrm{I}}^{(1)}\right) \\ &\quad - \frac{1}{2}\mathrm{Re}\left(\left(\boldsymbol{\beta}_{i,\mathrm{I}}^{(1)}\otimes\boldsymbol{\alpha}_{i,\mathrm{I}}^{(1)}\right)^{\mathrm{T}}\tilde{\boldsymbol{R}}_{\mathrm{n}}\left(\boldsymbol{\beta}_{i,\mathrm{I}}^{(1)}\otimes\boldsymbol{\alpha}_{i,\mathrm{I}}^{(1)}\right)\right), \end{aligned} \tag{43}$$

where $\boldsymbol{R}_{\mathrm{n}} = \mathbb{E}\{\mathrm{vec}\{\boldsymbol{\mathcal{N}}\}\cdot\mathrm{vec}\{\boldsymbol{\mathcal{N}}\}^{\mathrm{H}}\}$, while $\mathrm{vec}\{\boldsymbol{\mathcal{N}}\} = \mathrm{vec}\{[\boldsymbol{\mathcal{N}}]_{(3)}^{\mathrm{T}}\} = \mathrm{vec}\{[\boldsymbol{\mathcal{N}}]_{(1)}\} \in \mathbb{C}^{M_1M_2N}$, and $\tilde{\boldsymbol{R}}_{\mathrm{n}} = \mathbb{E}\{\mathrm{vec}\{\boldsymbol{\mathcal{N}}\}\cdot\mathrm{vec}\{\boldsymbol{\mathcal{N}}\}^{\mathrm{T}}\}$. Additionally, we used the property $\mathrm{Im}(z)\,\mathrm{Im}(z) = \frac{1}{2}\mathrm{Re}(zz^*) - \frac{1}{2}\mathrm{Re}(zz)$ that is valid for any complex number $z\in\mathbb{C}$.

The variance of the second term can be written as

$$\begin{aligned}\mathbb{E}\left\{\left(\Delta\mu_{i,\mathrm{II}}^{(1)}\right)^2\right\} &= \frac{1}{2}\left(\boldsymbol{\beta}_{i,\mathrm{II}}^{(1)}\otimes\boldsymbol{\alpha}_{i,\mathrm{II}}^{(1)}\right)^{\mathrm{H}}\boldsymbol{R}_{\mathrm{n}}^{*}\left(\boldsymbol{\beta}_{i,\mathrm{II}}^{(1)}\otimes\boldsymbol{\alpha}_{i,\mathrm{II}}^{(1)}\right) \\ &\quad - \frac{1}{2}\mathrm{Re}\left(\left(\boldsymbol{\beta}_{i,\mathrm{II}}^{(1)}\otimes\boldsymbol{\alpha}_{i,\mathrm{II}}^{(1)}\right)^{\mathrm{T}}\tilde{\boldsymbol{R}}_{\mathrm{n}}\left(\boldsymbol{\beta}_{i,\mathrm{II}}^{(1)}\otimes\boldsymbol{\alpha}_{i,\mathrm{II}}^{(1)}\right)\right). \end{aligned} \tag{44}$$

The correlation between terms is given by

$$\begin{aligned}2\cdot\mathbb{E}\left\{\Delta\mu_{i,\mathrm{I}}^{(1)}\Delta\mu_{i,\mathrm{II}}^{(1)}\right\} &= \left(\boldsymbol{\beta}_{i,\mathrm{I}}^{(1)}\otimes\boldsymbol{\alpha}_{i,\mathrm{I}}^{(1)}\right)^{\mathrm{H}}\boldsymbol{R}_{\mathrm{n}}^{*}\left(\boldsymbol{\beta}_{i,\mathrm{II}}^{(1)}\otimes\boldsymbol{\alpha}_{i,\mathrm{II}}^{(1)}\right) \\ &\quad - \mathrm{Re}\left(\left(\boldsymbol{\beta}_{i,\mathrm{I}}^{(1)}\otimes\boldsymbol{\alpha}_{i,\mathrm{I}}^{(1)}\right)^{\mathrm{T}}\tilde{\boldsymbol{R}}_{\mathrm{n}}\left(\boldsymbol{\beta}_{i,\mathrm{II}}^{(1)}\otimes\boldsymbol{\alpha}_{i,\mathrm{II}}^{(1)}\right)\right). \end{aligned} \tag{45}$$

In general, we need to evaluate the expressions (43) and (44) to find a good enough description for the performance of the i-th spatial frequency in the 1-mode. Note that we can derive closed-form expressions if we impose additional assumptions on the noise statistics.

B. SPECIAL CASE OF ZMCSCG NOISE

To this end, we assume that the elements of the tensor $\boldsymbol{\mathcal{N}}$ are independent and are drawn from a zero mean circularly symmetric complex Gaussian (ZMCSCG) distribution with variance σ_{n}^2. Then the covariance matrix turns into $\boldsymbol{R}_{\mathrm{n}} = \sigma_{\mathrm{n}}^2\boldsymbol{I}_{MN}$, while $\tilde{\boldsymbol{R}}_{\mathrm{n}} = \boldsymbol{0}$. In this case, the updated expressions for the components of the MSE are given by

$$\mathbb{E}\left\{\left(\Delta\mu_{i,\mathrm{I}}^{(1)}\right)^2\right\} = \frac{\sigma_{\mathrm{n}}^2}{2}\cdot\mathbb{E}\left\{\left\|\boldsymbol{\alpha}_{i,\mathrm{I}}^{(1)}\right\|_2^2\left\|\boldsymbol{\beta}_{i,\mathrm{I}}^{(1)}\right\|_2^2\right\}, \tag{46}$$

$$\mathbb{E}\left\{\left(\Delta\mu_{i,\mathrm{II}}^{(1)}\right)^2\right\} = \frac{\sigma_{\mathrm{n}}^2}{2}\cdot\mathbb{E}\left\{\left\|\boldsymbol{\alpha}_{i,\mathrm{II}}^{(1)}\right\|_2^2\left\|\boldsymbol{\beta}_{i,\mathrm{II}}^{(1)}\right\|_2^2\right\}. \tag{47}$$

The updated expression for the cross-mode component of the MSE is given by

$$\begin{aligned}&2\cdot\mathbb{E}\left\{\Delta\mu_{i,\mathrm{I}}^{(1)}\Delta\mu_{i,\mathrm{II}}^{(1)}\right\} \\ &\quad = \sigma_{\mathrm{n}}^2\cdot\mathbb{E}\left\{\left(\boldsymbol{\beta}_{i,\mathrm{I}}^{(1)}\otimes\boldsymbol{\alpha}_{i,\mathrm{I}}^{(1)}\right)^{\mathrm{H}}\left(\boldsymbol{\beta}_{i,\mathrm{II}}^{(1)}\otimes\boldsymbol{\alpha}_{i,\mathrm{II}}^{(1)}\right)\right\}. \end{aligned} \tag{48}$$

C. FURTHER SIMPLIFICATIONS

The current expressions for the parameters $\boldsymbol{\beta}_{i,\mathrm{I}}^{(1)}$ and $\boldsymbol{\beta}_{i,\mathrm{II}}^{(1)}$ include the instantaneous realization of the source signal snapshots $\boldsymbol{S}$. In this part, we eliminate and replace them with the signal covariance matrix

$$\left\|\boldsymbol{\beta}_{i,\mathrm{I}}^{(1)}\right\|_2^2 = \boldsymbol{e}_i^{\mathrm{T}}\left(\boldsymbol{S}^{\mathrm{H}}\right)^{+}\left(\boldsymbol{S}\right)^{+}\boldsymbol{e}_i = \frac{1}{N}\boldsymbol{e}_i^{\mathrm{T}}\hat{\boldsymbol{R}}_{\mathrm{s}}^{-1}\boldsymbol{e}_i, \tag{49}$$

where $\hat{\boldsymbol{R}}_{\mathrm{s}} = \frac{1}{N}\boldsymbol{S}\boldsymbol{S}^{\mathrm{H}}$. Also, we can write

$$\begin{aligned}\left\|\boldsymbol{\beta}_{i,\mathrm{II}}^{(1)}\right\|_2^2 &= \boldsymbol{e}_i^{\mathrm{T}}\left(\boldsymbol{S}^{\mathrm{T}}\diamond\frac{1}{\sqrt{M_2}}\boldsymbol{A}^{(2)}\right)^{+}\left(\boldsymbol{S}^{\mathrm{T}}\diamond\frac{1}{\sqrt{M_2}}\boldsymbol{A}^{(2)}\right)^{+\mathrm{H}}\boldsymbol{e}_i \\ &= \boldsymbol{e}_i^{\mathrm{T}}\left(\boldsymbol{S}^{*}\boldsymbol{S}^{\mathrm{T}}\odot\frac{1}{M_2}\boldsymbol{A}^{(2)\mathrm{H}}\boldsymbol{A}^{(2)}\right)^{-1}\boldsymbol{e}_i \\ &= \frac{1}{N}\boldsymbol{e}_i^{\mathrm{T}}\left(\hat{\boldsymbol{R}}_{\mathrm{s}}^{*}\odot\frac{1}{M_2}\boldsymbol{A}^{(2)\mathrm{H}}\boldsymbol{A}^{(2)}\right)^{-1}\boldsymbol{e}_i. \end{aligned} \tag{50}$$

Following [13] (therein the Section 5b) we can show that

$$\mathbb{E}\left\{\left\|\boldsymbol{\beta}_{i,\mathrm{I}}^{(1)}\right\|_2^2\right\} = \frac{1}{N}\boldsymbol{e}_i^{\mathrm{T}}\boldsymbol{R}_{\mathrm{s}}^{-1}\boldsymbol{e}_i, \tag{51}$$

$$\mathbb{E}\left\{\left\|\boldsymbol{\beta}_{i,\mathrm{II}}^{(1)}\right\|_2^2\right\} = \frac{1}{N}\boldsymbol{e}_i^{\mathrm{T}}\left(\boldsymbol{R}_{\mathrm{s}}^{*}\odot\frac{1}{M_2}\boldsymbol{A}^{(2)\mathrm{H}}\boldsymbol{A}^{(2)}\right)^{-1}\boldsymbol{e}_i. \tag{52}$$

Furthermore, we omit the conjugate of the covariance matrix $\boldsymbol{R}_{\mathrm{s}}$ since we are interested only in the diagonal entries of the corresponding inverse that are real-valued.

D. FINAL EXPRESSIONS

The resulting MSE of the i-th spatial frequency in the 1-mode of 2-D Tensor ESPRIT comprises two terms

$$\mathrm{MSE}_{\mathrm{STE}}{}_{i}^{(1)} = \mathrm{MSE}_{\mathrm{STE}}{}_{i,\mathrm{I}}^{(1)} + \mathrm{MSE}_{\mathrm{STE}}{}_{i,\mathrm{II}}^{(1)}, \tag{53}$$

The term $\mathrm{MSE}_{\mathrm{STE}}{}_{i,\mathrm{I}}^{(1)}$ in (54) shown at the bottom of this page, describes the error caused by the perturbations of the original signal subspace (23) and $\mathrm{MSE}_{\mathrm{STE}}{}_{i,\mathrm{II}}^{(1)}$ in (55) shown at the bottom of this page, corresponds to the error caused by the perturbations in the 1-mode (30). Additionally, following the analogous derivations as in [14], it can be shown that the MSE for 2-D ESPRIT [15] can be written as in (56) shown at the bottom of this page. We use it as a reference for the simulation results. We use the following parameters and quantities for the provided expressions: $\boldsymbol{R}_{\mathrm{s}}$ is the signal covariance matrix, $\boldsymbol{A}^{(r)}$ is the steering matrix in the r-th mode, $\boldsymbol{e}_i$ is the i-th unit vector, $\boldsymbol{\mathcal{L}}_i^{(1)}$ is defined in (22), and $\boldsymbol{T}^{(r)}$ comes from (6).

E. DISCUSSION

Observing the resulting expressions for the MSE, we can notice additional projections onto each mode in (54) in comparison to (56) that reduces the norm of $[\boldsymbol{\mathcal{L}}_i^{(1)}]_{(3)}$ which belongs to the left-nullspace of $\boldsymbol{A}$. Additionally, the expression (52) contains the elementwise product with the matrix $\frac{1}{M_2}\boldsymbol{A}^{(2)\mathrm{H}}\boldsymbol{A}^{(2)}$ in contrast to (51) which provides the reason for the resistance against the impact of correlation for (55) (even if $\boldsymbol{R}_{\mathrm{s}}$ is rank deficient), especially for spatially separated sources. We can explain it by noticing that for spatially separated sources, the product $\boldsymbol{A}^{(2)\mathrm{H}}\boldsymbol{A}^{(2)}$ is approximately a diagonal matrix. As a result, the condition number of the product $\boldsymbol{R}_{\mathrm{s}}\odot\frac{1}{M_2}\boldsymbol{A}^{(2)\mathrm{H}}\boldsymbol{A}^{(2)}$ will be reduced in comparison to the condition number of the matrix $\boldsymbol{R}_{\mathrm{s}}$ only.

VI. SIMULATION RESULTS

In this section, we present selected simulation results to demonstrate the validity of the derived expressions for the performance analysis.

We analyze the derived expressions of the performance analysis and compare them to the curves obtained via Monte Carlo trials to verify the obtained results. For all the simulation results, the red lines correspond to the performance analysis of the 2-D Standard ESPRIT algorithm (`SE`), the blue lines describe the behavior of 2-D Standard Tensor ESPRIT (`STE`), and the gray lines are the various error components in (42). All the curves obtained via Monte Carlo trials are given as solid lines and depicted with "`em`". The analytical expressions are represented with dashed lines and the label "`an`". The analytical performance of 2-D Standard ESPRIT is computed with the expression (56), and the analysis of 2-D Standard Tensor ESPRIT is based on (53), (54), and (55). We label the first MSE component (54) that is caused by the perturbation of the signal subspace itself (23) as "`core`". Moreover, we label the second MSE component (55), which is caused by the perturbation of the corresponding projection matrix in every mode (30) as "`mode`". The impact of the cross product between two error terms (29) and (37) on the MSE is denoted as "`cross`" and is computed based on the expression (48). We use the root mean squared error (RMSE) to quantify the overall performance and the impact on each individual component in (42). The overall RMSE is calculated using the expression

$$\mathrm{RMSE} = \sqrt{\mathbb{E}\left\{\frac{1}{2d}\sum_{r=1}^{2}\sum_{i=1}^{d}\left(\mu_i^{(r)}-\hat{\mu}_i^{(r)}\right)^2\right\}}. \tag{57}$$

Each Monte Carlo result was obtained by averaging over 10,000 realizations of the noise.

We denote the correlation coefficient between modes as ρ and use it to create the source signal correlation matrix as

$$\boldsymbol{R}_{\mathrm{s}} = \rho\mathbf{1} + (1-\rho)\boldsymbol{I}_d, \tag{58}$$

where $\mathbf{1}\in\mathbb{R}^{d\times d}$ is a matrix of ones. We calculate the noise variance as a function of the SNR, i.e., $\sigma_n^2 = 10^{-\frac{\mathrm{SNR}}{10}}$. The location of each individual spatial frequency $\mu_i^{(r)}$ is sampled from a uniform distribution on the interval $(-\pi,\pi]$ and then fixed for all Monte Carlo trials. For the presented simulation results, we use the following realization of spatial frequencies

$$\mathrm{MSE}_{\mathrm{STE}}{}_{i,\mathrm{I}}^{(1)} = \frac{\sigma_{\mathrm{n}}^2}{2N}\left(\boldsymbol{R}_{\mathrm{s}}^{-1}\right)_{i,i}\cdot\left\|\left[\boldsymbol{\mathcal{L}}_i^{(1)}\right]_{(3)}\left(\boldsymbol{T}^{(2)}\otimes\boldsymbol{T}^{(1)}\right)\right\|_2^2 \tag{54}$$

$$\mathrm{MSE}_{\mathrm{STE}}{}_{i,\mathrm{II}}^{(1)} = \frac{\sigma_{\mathrm{n}}^2}{2N}\left(\left(\boldsymbol{R}_{\mathrm{s}}\odot\frac{1}{M_2}\boldsymbol{A}^{(2)\mathrm{H}}\boldsymbol{A}^{(2)}\right)^{-1}\right)_{i,i}\cdot\left\|\boldsymbol{e}_i^{\mathrm{T}}\frac{1}{\sqrt{M_2}}\boldsymbol{A}^{(2)\mathrm{T}}\left[\boldsymbol{\mathcal{L}}_i^{(1)}\right]_{(1)}\left(\boldsymbol{I}_{M_1}-\boldsymbol{T}^{(1)}\right)\right\|_2^2 \tag{55}$$

$$\mathrm{MSE}_{\mathrm{SE}}{}_{i}^{(1)} = \frac{\sigma_{\mathrm{n}}^2}{2N}\left(\boldsymbol{R}_{\mathrm{s}}^{-1}\right)_{i,i}\cdot\left\|\left[\boldsymbol{\mathcal{L}}_i^{(1)}\right]_{(3)}\right\|_2^2,\quad\text{where}\quad\left[\boldsymbol{\mathcal{L}}_i^{(1)}\right]_{(3)} = \boldsymbol{e}_i^{\mathrm{T}}\left(\left(\tilde{\boldsymbol{J}}_2^{(1)}\boldsymbol{A}\right)^{+}\tilde{\boldsymbol{J}}_2^{(1)}-\left(\tilde{\boldsymbol{J}}_1^{(1)}\boldsymbol{A}\right)^{+}\tilde{\boldsymbol{J}}_1^{(1)}\right) \tag{56}$$

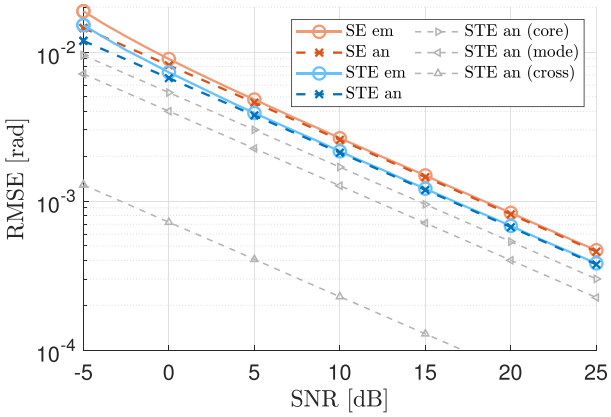

(a) RMSE versus SNR.

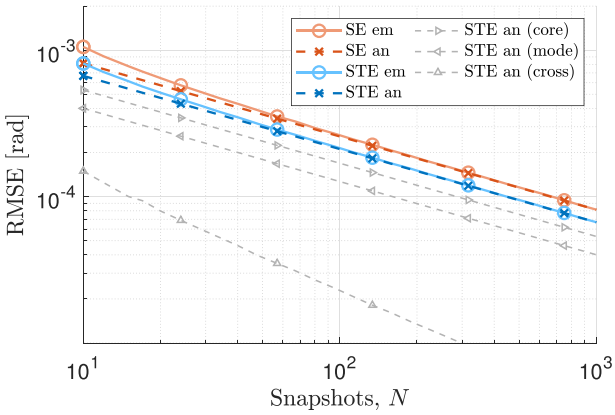

(b) RMSE versus number of snapshots.

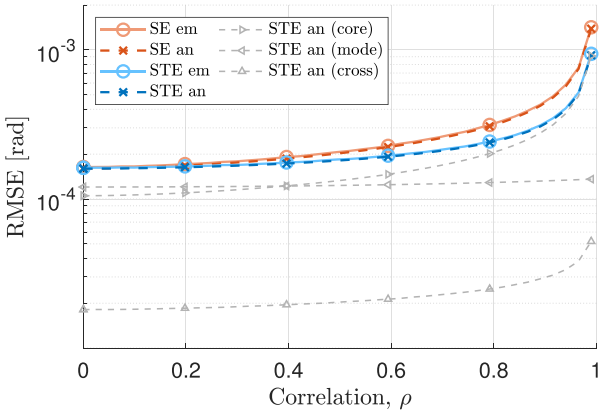

(c) RMSE versus correlation.

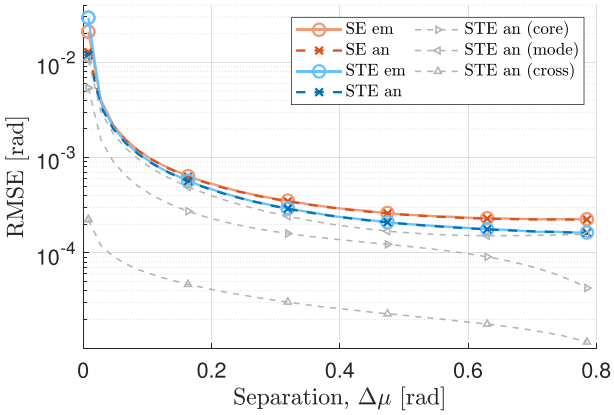

(d) RMSE versus spatial separation.

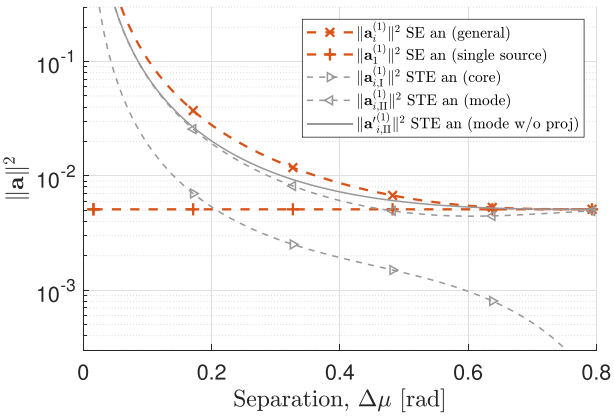

(e) $\|\boldsymbol{\alpha}\|^2$ versus spatial separation for the 1-mode

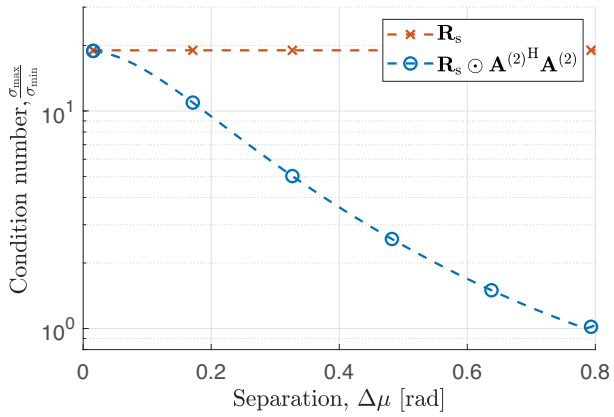

(f) Condition number versus spatial separation for the 1-mode

FIGURE 1. Performance analysis for 2-D Tensor ESPRIT in terms of physical parameters.

(modes × sources)

$$\boldsymbol{\mu} = \begin{bmatrix} -3.13 & 0.99 & 0.55 & -0.59 \\ 2.27 & 1.18 & -0.86 & -0.40 \end{bmatrix} \in \mathbb{R}^{R \times d}, \quad (59)$$

unless otherwise stated. The key simulation parameters for each figure can be found in Table 1. In Fig. 1(a), we depict

TABLE 1. Simulation Parameters

Figure	Parameters				
1(a)	$M = [8, 8]$	$N = 100$	-	$d = 4$	$\rho = 0.7$
1(b)	$M = [8, 8]$	-	SNR $= 30$ dB	$d = 4$	$\rho = 0.7$
1(c)	$M = [8, 8]$	$N = 100$	SNR $= 30$ dB	$d = 4$	-
1(d)	$M = [8, 8]$	$N = 100$	SNR $= 30$ dB	$d = 2$	$\rho = 0.7$
1(e)	$M = [8, 8]$	-	-	$d = 2$	$\rho = 0.7$
1(f)	$M = [8, 8]$	-	-	$d = 2$	$\rho = 0.7$

the impact of the SNR on the resulting RMSE and the MSE components. We can see that all the error components decrease linearly on a logarithmic scale. We can notice that STE has a better performance in comparison to SE due to a better performance for correlated sources.

In Fig. 1(b), we can observe the impact of the number of snapshots on the resulting error and its individual parts. Tensor ESPRIT outperforms Standard ESPRIT due to a better ability to handle correlated signals. We notice that the error for the cross-product component has a steeper dependency on the number of snapshots and decreases faster. Based on this observation, we exclude the cross-product component from consideration and the resulting expressions for the MSE of the i-th source in the r-mode.

In Fig. 1(c), we depict the dependency of MSE on the correlation between two sources. The contributions of each error component can be seen. We can notice that the "mode" error component has a smaller dependency on the correlation due to its structure given in (55), where the Hadamard product helps to decorrelate the covariance matrix via the element-wise product with $\frac{1}{M_r}\boldsymbol{A}^{(r)\mathrm{H}}\boldsymbol{A}^{(r)}$, $\forall r \in \{1, 2\}$ and reduces the condition number of the result. We show the corresponding simulation results for the 1-mode in Fig. 1(f). It presents the condition numbers as a function of the spatial separation between two sources $\mu_1^{(r)} = 0$ and $\mu_2^{(r)} = \Delta\mu^{(r)}, \forall r = \{1, 2\}$ for the matrix $\boldsymbol{R}_\mathrm{s}$ and for the product $\boldsymbol{R}_\mathrm{s} \odot \frac{1}{M_2}\boldsymbol{A}^{(2)\mathrm{H}}\boldsymbol{A}^{(2)}$ assuming a correlation of $\rho = 0.7$. We can conclude that for the spatially separated sources, when $\Delta\mu_r \geq \frac{2\pi}{M_r}$, $\forall r = \{1, 2\}$ the impact of correlation to the "mode" component can be neglected. As a result, further analyzing the simulations in Fig. 1(c), we can say that for the region of high correlation, the "mode" component (55) less dependent on the correlation, while the "core" component (54) has similar behavior to Standard ESPRIT but it is lower due to the additional projections in (54). At the same time, such projection helps to reduce the impact of spatial separation on the "core" component, as we will see in Fig. 1(d). On the contrary, we can also observe that for the region of small values of correlation, Tensor ESPRIT has a similar overall performance as Standard ESPRIT.

In Fig. 1(d), we analyze the impact of the source separation on the performance. In this simulation, we consider two sources $\mu_1^{(r)} = 0$ and $\mu_2^{(r)} = \Delta\mu^{(r)}$, $\forall r = \{1, 2\}$. The total range is equal to $\Delta\mu^{(r)} \in [0, \frac{2\pi}{M_r}]$. We notice that the impact of the "core" part of the error substantially decreases with an increase in the source separation, where the "mode" component has the dominant impact on the MSE.

In Fig. 1(e) we compare various $\|\boldsymbol{\alpha}\|_2^2$ terms for the 1-mode. In general, the parameter $\boldsymbol{\alpha}$ characterizes the error of the signal subspace estimation as a function of spatial separation. For this particular figure, we present $\boldsymbol{\alpha}_i^{(1)\mathrm{T}} = [\boldsymbol{\mathcal{L}}_i^{(1)}]_{(3)}$ in (16) for Standard ESPRIT, and the "core" and "mode" error components of Tensor ESPRIT in (28) and (35), correspondingly. Additionally, we can show that the norm of $\boldsymbol{\alpha}_i^{(1)}$ for a single source using Standard ESPRIT is equal to

$$\left\|\boldsymbol{\alpha}_1^{(1)}\right\|_2^2 = \frac{2}{\left(M_1 - 1\right)^2 M_2}. \tag{60}$$

We use it as a reference line that does not depend on spatial separation and where we do not need to calculate the pseudoinverse as in (16). Using a solid gray line, we show the performance without the projection onto the left-nullspace of $\boldsymbol{A}^{(1)}$ in the "mode" component (35)

$$\boldsymbol{\alpha}'^{(1)\mathrm{T}}_{i,\mathrm{II}} = \boldsymbol{e}_i^\mathrm{T} \frac{1}{\sqrt{M_2}} \boldsymbol{A}^{(2)\mathrm{T}} \left[\boldsymbol{\mathcal{L}}_i^{(1)}\right]_{(1)}. \tag{61}$$

We can observe that the "core" component has a much smaller dependency on the spatial separation due to an additional projection to the signal subspace in each mode. On the other hand, we can see that $\boldsymbol{\alpha}_{i,\mathrm{II}}^{(1)}$ for the "mode" component also has a smaller norm than $\boldsymbol{\alpha}_i^{(1)}$ for Standard ESPRIT because of its structure, which comprises the product with $\boldsymbol{A}^{(2)}$ and the projection onto the left-nullspace of $\boldsymbol{A}^{(1)}$. Finally, we can notice that the performance difference between Standard ESPRIT and Tensor ESPRIT vanishes for spatially separated sources. There, the error is mostly dominated by the "mode" component of Tensor ESPRIT.

Overall, the presented simulation results confirm that the derived expressions for the performance analysis reflect the behavior of 2-D Tensor ESPRIT. Additionally, the simulation results show that the cross-product term (48) between different error terms can be dropped, which further simplifies the MSE expression.

VII. CONCLUSION

In this paper, we present a performance analysis of 2-D Tensor ESPRIT in terms of physical parameters. We show that the error in the r-mode depends only on two perturbation components, irrespective of the dimensionality of the original problem. The provided closed-form expressions do not rely on the intermediate quantities from the HOSVD and have better tractability. Compared to previously reported works on perturbation analysis, we get a simpler expression that can be directly utilized to evaluate the performance of ESPRIT-type algorithms. The derived results can be applied on the system level to optimize the system parameters.

REFERENCES

[1] D. Rakhimov, J. Zhang, A. L. F. de Almeida, A. Nadeev, and M. Haardt, "Channel estimation for hybrid multi-carrier mmWave MIMO systems using 3-D unitary Tensor-ESPRIT in DFT beamspace," in *Proc. 53rd Asilomar Conf. Signals, Syst., Comput.*, 2019, pp. 447–451.

[2] J. Zhang, D. Rakhimov, and M. Haardt, "Gridless channel estimation for hybrid mmWave MIMO systems via Tensor-ESPRIT algorithms in DFT beamspace," *IEEE J. Sel. Topics Signal Process.*, vol. 15, no. 3, pp. 816–831, Apr. 2021.

[3] F. Li, H. Liu, and R. J. Vaccaro, "Performance analysis for DOA estimation algorithms: Unification, simplification, and observations," *IEEE Trans. Aerosp. Electron. Syst.*, vol. 29, no. 4, pp. 1170–1184, Oct. 1993.

[4] F. Roemer, H. Becker, M. Haardt, and M. Weis, "Analytical performance evaluation for HOSVD-based parameter estimation schemes," in *Proc. 3rd IEEE Int. Workshop Comput. Adv. Multi-Sensor Adaptive Process.*, 2009, pp. 77–80.

[5] F. Roemer, H. Becker, and M. Haardt, "Analytical performance assessment for multi-dimensional Tensor-ESPRIT-type parameter estimation algorithms," in *Proc. IEEE Int. Conf. Acoust., Speech Signal Process.*, 2010, pp. 2598–2601.

[6] F. Roemer, M. Haardt, and G. Del Galdo, "Analytical performance assessment of multi-dimensional matrix- and tensor-based ESPRIT-Type algorithms," *IEEE Trans. Signal Process.*, vol. 62, no. 10, pp. 2611–2625, May 2014.

[7] J. Steinwandt, F. Roemer, and M. Haardt, "Analytical performance assessment of ESPRIT-type algorithms for coexisting circular and strictly non-circular signals," in *Proc. IEEE Int. Conf. Acoust., Speech Signal Process.*, 2016, pp. 2931–2935.

[8] J. Steinwandt, F. Roemer, and M. Haardt, "Analytical performance evaluation of multi-dimensional Tensor-ESPRIT-based algorithms for strictly non-circular sources," in *Proc. IEEE Sensor Array Multichannel Signal Process. Workshop*, 2016, pp. 1–5.

[9] M. Haardt, F. Roemer, and G. Del Galdo, "Higher-order SVD-Based subspace estimation to improve the parameter estimation accuracy in multidimensional harmonic retrieval problems," *IEEE Trans. Signal Process.*, vol. 56, no. 7, pp. 3198–3213, Jul. 2008.

[10] M. Haardt and J. A. Nossek, "Unitary ESPRIT: How to obtain increased estimation accuracy with a reduced computational burden," *IEEE Trans. Signal Process.*, vol. 43, no. 5, pp. 1232–1242, May 1995.

[11] F. Li and R. J. Vaccaro, "Unified analysis for DOA estimation algorithms in array signal processing," *Signal Process.*, vol. 25, no. 2, pp. 147–169, Nov. 1991.

[12] T. G. Kolda and B. W. Bader, "Tensor decompositions and applications," *SIAM Rev.*, vol. 51, no. 3, pp. 455–500, 2009.

[13] D. Rakhimov and M. Haardt, "Analytical performance assessment of 1-D ESPRIT in DFT beamspace in terms of physical parameters," in *Proc. 57th Asilomar Conf. Signals, Syst., Comput.*, 2023, pp. 1–7.

[14] F. Li, H. Liu, and R. Vaccaro, "Performance analysis for DOA estimation algorithms using physical parameters," in *Proc. Int. Conf. Acoust., Speech, Signal Process.*, 1992, pp. 537–540.

[15] M. Haardt, M. D. Zoltowski, C. P. Mathews, and J. Nossek, "2D unitary ESPRIT for efficient 2D parameter estimation," in *Proc. Int. Conf. Acoust., Speech, Signal Process.*, 1995, pp. 2096–2099.